Available online at www.sciencedirect.com
ScienceDirect
ELSEVIER
C. R. Physique 8 (2007) 1174–1183
COMPTES RENDUS PHYSIQUE
http://france.elsevier.com/direct/COMREN/

Optical parametric sources for the infrared/Sources optiques paramétriques pour l'infrarouge

Large intrinsic birefringence in zinc-blende based artificial semiconductors

Jean-Marc Jancu, Jean-Christophe Harmand, Gilles Patriarche, Anne Talneau, Karine Meunier, Frank Glas, Paul Voisin *

LPN–CNRS, route de Nozay, 91460 Marcoussis, France

Available online 26 October 2007

Abstract

A new attempt to solve the phase matching problem for semiconductor-based frequency conversion devices, based on the implementation of intrinsic birefringence in artificial materials, is discussed. The first results concerning the growth and characterization of ultrashort period superlattices are presented. ***To cite this article: J.-M. Jancu et al., C. R. Physique 8 (2007).***
© 2007 Académie des sciences. Published by Elsevier Masson SAS. All rights reserved.

Résumé

Biréfringence intrinsèque dans des semiconducteurs artificiels. Nous décrivons une tentative originale pour résoudre le problème de l'accord de phase pour la conversion de fréquences optiques dans des composants semiconducteurs. La possibilité d'implémenter une grande biréfringence intrinsèque dans des semiconducteurs artificiels basés sur des composés ayant la structure cubique de la blende de zinc est d'abord discutée théoriquement. Les premiers résultats concernant la croissance épitaxiale et la caractérisation optique de superréseaux d'ultracourte période sont présentés ensuite. ***Pour citer cet article : J.-M. Jancu et al., C. R. Physique 8 (2007).***
© 2007 Académie des sciences. Published by Elsevier Masson SAS. All rights reserved.

Keywords: Optical materials; Non-linear optics; Semiconductor nanostructures

Mots-clés : Matériaux pour l'optique ; Optique non-linéaire ; Nanostructures semiconductrices

1. Introduction

Zinc-blende based semiconductors have many favorable characteristics that make them good candidates for applications in integrated non-linear optics. They indeed combine high material quality, large second order susceptibilities, mature technology (in particular for guided-wave optics), and availability of powerful, integrable pump lasers. During the last decade, these promises have driven many attempts to solve the remaining, tantalizing problem of phase matching for efficient and flexible optical frequency conversion [1]. Most successful approaches, so far, are based on quasi-phase matching scenarios using state of the art technological tricks. Here, we report on a different attempt based on a direct implementation of large birefringence in novel, man-made semiconductors based on III–V or II–VI

* Corresponding author.
E-mail address: Paul.Voisin@lpn.cnrs.fr (P. Voisin).

1631-0705/$ – see front matter © 2007 Académie des sciences. Published by Elsevier Masson SAS. All rights reserved.
doi:10.1016/j.crhy.2007.09.005

materials. The driving idea is that ultrashort period superlattices of highly strained materials sharing no-common atom would present a strongly anisotropic unit cell [2], leading to anisotropic optical properties and possibly to enhanced second order non-linearities. Given the large span of possibilities and the difficulty of optimizing growth parameters for new, highly strained materials, the only solution is a modeling-driven approach. This consideration defines the methodological roadmap: to fulfill the ambitious goal of pre-evaluating the optical properties of artificial materials, one should be able to calculate with high reliability and precision the dielectric function and piezo-optic constants of bulk materials, and to extend the calculation to heterostructures. This is an open theoretical challenge in solid state physics. In the first part of this article we prove that the extended basis spds* tight-binding method [3] passes these three prerequisites. In fact, it is so far the only theoretical approach that fulfills the needs of this project. After numerical exploration of a large number of material combinations, an astonishingly simple practical conclusion is reached: the birefringence of an ultrashort-period superlattice (USPSL) is approximately the layer-per-layer average of the different material piezobirefringences. As large differences are observed in bulk piezo-optic constants, it becomes possible to design strain-compensated structures with large native birefringence up to $\delta n \approx 0.06$. We then discuss practical implementation of this engineering 'rule of thumb' in exotic man-made semiconductors, delineate the problems associated with such ultimate epitaxy of highly strained ultrathin heterolayers of materials sharing no-common atom, and finally prove the successful growth of InGaAs–AlP ultrashort period superlattices.

2. Symmetry considerations

As sketched in Fig. 1, the atomic arrangement at a (001) interface between materials C1A1 and C2A2 ('C' and 'A' standing for cation and anion species, respectively) reveals a major symmetry breakdown which was studied and explained only in the mid-1990s [4–8]: the presence of the interface breaks not only the translational invariance along the growth axis, but also an element of rotational symmetry, as the bonds lying in the (110) and (-110) planes differ in the unit cell forming the interface itself. Among the missing symmetry elements of the zinc blende structure is the $\pi/2$ roto-inversion symmetry around the (001) axis. The resulting point-group symmetry named C2v contains only the mirror reflexion planes (110) and (-110). Obviously, in the interface cell, the three directions, $X' \equiv [110]$, $Y' \equiv [-110]$, and $Z \equiv [001]$ differ. When considering not a single interface but a quantum well or a superlattice, it may happen that a higher symmetry is restored: this is the case when the materials share a common atom, for instance the anion in GaAs/AlAs. In such heterostructures, interfaces transform into each other by the $\pi/2$ roto-inversion centered on an atomic site in the middle of the well. The point group symmetry becomes D2d, and the in-plane directions X' and Y' are equivalent (and of course differ from the growth direction Z). Note that in presence of asymmetrical chemical composition gradients, the C2v symmetry prevails even in a common atom system, and that application of an external electric field along the growth direction allows a tunable lowering of the symmetry from D2d to C2v.

It is noteworthy, when both the cations C1 and C2 and the anions A1 and A2 differ, the interfaces involve specific chemical bonds (A1–C2 or A2–C1) that do not exist in the host materials. Generally, these interface bonds are strongly strained even if the bulk constituents are lattice-matched. A typical example of such a situation is the InAs/AlSb system (see Fig. 1), nearly lattice-matched to GaSb, where nominal interfaces involve In–Sb and Al–As

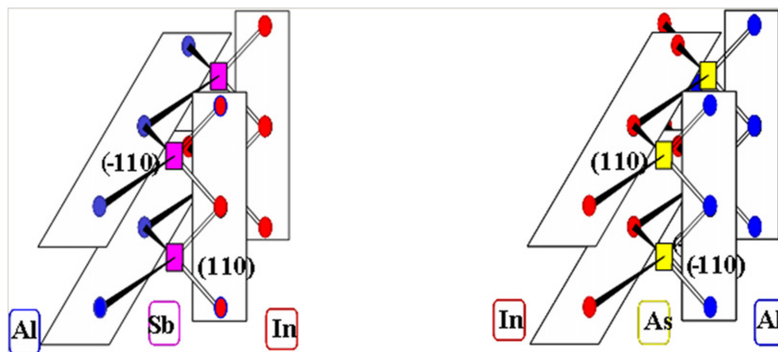

Fig. 1. Sketch of the chemical bond arrangement at InAs/AlSb and AlSb/InAs interfaces. Planes of specific, highly strained interface bonds lying in the (110) plane exist at each interface, In–Sb and Al–As, respectively.

bonds, respectively much longer and shorter than the bulk bonds. Another interesting situation is met in some strained layer heterostructures where bulk bonds are strained symmetrically with respect to the substrate and interface bonds are unstrained. This situation is found in the GaP–(GaIn)As system, where the free-standing lattice parameter is equal to the GaAs parameter, and the interface bonds are Ga–As and (GaIn)–P.

To conclude this section, we retain that semiconductor heterostructures have a reduced symmetry, either D2d or C2v, which allows for uniaxial or biaxial optical anisotropy, respectively. C2v symmetry manifests itself as a linear dichroism between polarizations X' and Y' near the fundamental absorption edge under normal incidence, while the main characteristic of D2d symmetry is the dichroism between Z and in-plane polarizations. In the latter case, the polarization anisotropy of optical transitions is observed in guided-wave optics and the related TE/TM anisotropy of optical index is combined with the 'geometrical' birefringence, due to the different interface boundary conditions of Z-polarized and in-plane polarized optical waves.

These symmetry considerations are quite general, but the related effects are usually small and spectrally limited to the near gap region in standard quantum wells (say for well thicknesses in the 5–20 nm range): in such a case, from the microscopic, quantum theory point of view, the D2d character is mainly due to the splitting of heavy (H) and light (L) holes and related optical selection rules, while the C2v character appears due to a mixing of heavy and light holes states by the interface potential. For this reason, to a first approximation, dichroism extends mostly over the spectral range between the H1–E1 and L1–E1 transitions. The dominant D2d character corresponds to 100% dichroism (heavy-hole transition forbidden in Z-polarization), while the C2v character produces dichroisms ranging from the percent range (asymmetric GaAs/AlGaAs quantum wells) up to 10–20% in no-common atom (InGa)As–InP quantum wells [4]. Values close to 100% have been observed, exceptionally, in type II, no-common atom interfaces such as BeTe/ZnSe [7]. These effects have been observed and analyzed in many different heterostructures in the late 1990s [4–8]. It is worth noting, in all these systems, that the anisotropy of optical index in the transparency region is well fitted with the Kramers–Kronig transform of the dichroism measured in a narrow (about 100 meV) spectral range near the absorption gap. This implies that about all the causality of this birefringence is contained in the near gap region, with little contribution from the upper lying transitions near the E1 and E2 gaps. Obviously, this index anisotropy is strongly resonant and does not extend far into the transparency region. As discussed below, this situation changes when reaching the regime of ultra-short period superlattices (USPSL) that behave as artificial bulk materials with a strongly anisotropic unit cell.

3. Calculations of the bulk dielectric function and piezo-optic constants

Clearly, the modeling of USPSL dielectric constants goes beyond the possibilities of k.p calculations and requires theoretical methods dealing with the full Brillouin zone and applicable to heterolayers. Empirical pseudopotentials (EPP), empirical tight binding (ETB) or ab-initio calculations can be envisionned for this purpose. Semi-empirical approaches give more easily a satisfactory description of excited states, and are much more efficient from the computational point of view. However, they are sensitive to parameterization issues. We have chosen here to focus on combinations of III–V semiconductors, where experimental data can be used for unambiguous empirical parameterizations. Electron band structure calculations were performed within the tight-binding approximation using an sp3d5s* nearest neighbor model that includes spin–orbit coupling [3]. This 40-band tight-binding model adequately reproduces, band parameters, chemical trends, and spectral functions of III–V semiconductors. This is illustrated in Fig. 2 which shows the calculated dielectric function (imaginary and real part) of GaAs, compared to the experimental data [9]. Optical response was considered within the independent particle approximation using a Peierls-coupling TB scheme that guarantees gauge invariance and charge conservation [10]. We use a mesh of 8200 points to sample the Brillouin zone and resulting discrete transitions are dressed with a 0.1 eV Gaussian broadening in order to get smooth spectra. The overall agreement is satisfactory especially in the static limit whereas electron–hole interactions account for the discrepancies near E1 and E2 critical points [11]. These results also apply to other compounds as shown in Table 1. Conversely, we found that current parameterizations of atomistic pseudopotentials fail in modeling dielectric constants [12], mainly due to a poor description of the Brillouin zone surface due to the limitation of the parameterization scheme [13]. Good agreement found in the literature for GaAs optical index using EPP [14] seems to result from compensation of errors in the calculated band structure and dipole moment [12].

Another prerequisite to realistic calculations of USPSL dielectric functions is an accurate description of the photoelastic response of material constituents. This is fully achieved within the present ETB approach for a large class

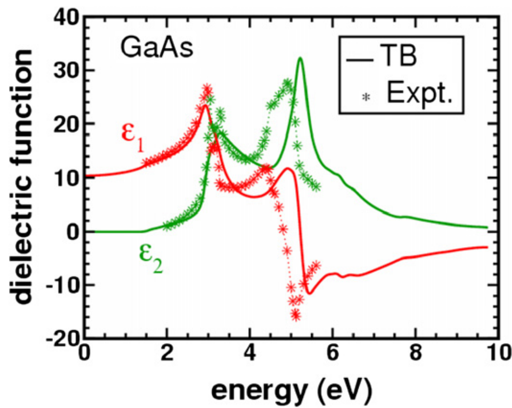

Fig. 2. Real and imaginary parts of GaAs dielectric function calculated using the spds* tight binding model, compared with the experimental spectra (Ref. [9]).

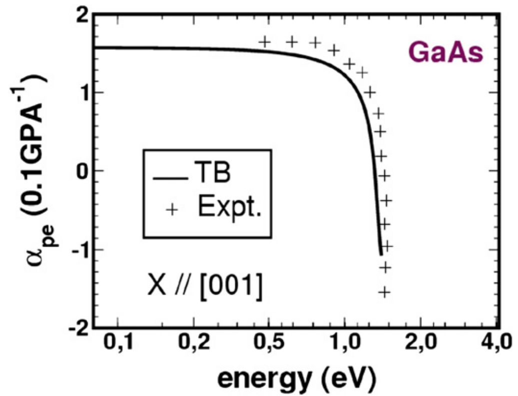

Fig. 3. Calculated dispersion of the piezo-optic constant in bulk GaAs, compared to experimental results (Ref. [9]).

Table 1
Calculated dielectric constant of cubic semiconductors, compared to experimental results (Ref. [9])

$\varepsilon 1(0)$	TB	Expt
Si	10.9	11.3
Ge	15.5	16.0
GaAs	10.5	10.9
AlAs	8.2	8.16
InAs	12.0	12.3

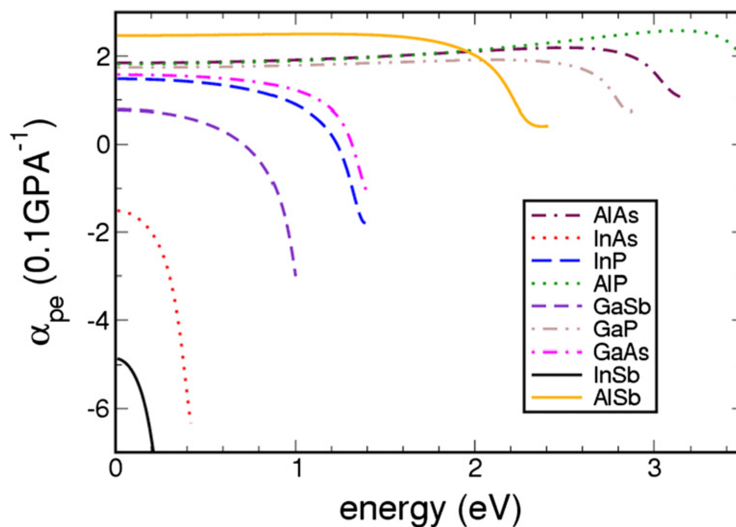

Fig. 4. Calculated dispersion of piezo-optic constants for the III–V semiconductors. Agreement with experiments is within 10%. Values in the long wavelength limit vary from below −2 to above +2.

of III–V semiconductors. The calculated and measured dispersions of piezo-optic constants in GaAs are compared in Fig. 3, and calculated dispersions for the main III–V semiconductors are shown in Fig. 4. Discrepancies with experimental data [9] are found to be less than 10% in the low-energy part of the spectra. In conclusion, the 40-band tight-binding model reproduces well the experiments reported in the literature. Most of deviations result from the non-inclusion of many-body effects, which corresponds to a systematic error (underestimate of optical index) of

about 2.5%. When extending the calculation to heterostructures, one should keep in mind another difficulty associated with local field effects. In the macroscopic limit, local fields are completely determined by the polarization dependent boundary conditions at the interface between two dielectrics, but obviously this does not hold in the microscopic limit which is actually difficult to handle. This issue was examined in Ref. [14] in the case of GaAs–AlGaAs USPSLs, and we retain that in the regime of ultrathin layers these effects can be neglected in a first approach.

4. Dielectric function in USPSLs

We first checked that in the case of GaAs/AlAs USPSLs we find a negligible optical anisotropy, essentially in agreement with Ref. [14]. From a microscopic symmetry point of view, this result reflects the fact that, owing to the nearly perfect lattice matching, the local environment of any metallic atom in the superlattice obeys the regular tetrahedral symmetry of the bulk. In the following, we focus on short-period [001]-oriented superlattices sharing no-common-atom, and more specifically on the two systems InAs/AlSb and (InGa)As/AlGaP. Fig. 5 shows the calculated real and imaginary dielectric functions of a InAs/AlSb 2/2 superlattice, for light polarized parallel (TM) and perpendicular (TE) to the SL growth direction. The in-plane lattice parameter is that of a GaSb substrate (6.0959 Å), actually different from the free-standing value (6.051 Å). Note that we use here classical elasticity to determine the atomic positions. We checked that using atomistic elasticity does not change significantly the results. The growth sequence is In–As=In–As=Al–Sb=Al–Sb=, where '=' and '–' indicate that corresponding chemical bonds lie in the X' and Y' planes, respectively. In the calculation, we use band offsets obtained from ab-initio calculations, that give fair agreement with known experimental values. A striking feature of the spectra is that optical anisotropy is distributed non-uniformly and shows sign oscillations throughout the absorption spectrum. This seemingly prohibits a simple, generic analysis of trends. Turning to the real part of the dielectric function, we observe a sizeable TE/TM optical anisotropy reflected by the difference between z and x' polarizations: $n_z - n_{x'} = \delta n_{z-x'} = -0.031$ in the long wavelength limit. A slightly different value is found for the other in-plane polarization: $n_z - n_{y'} = \delta n_{z-y'} = -0.019$. The in-plane anisotropy $\delta n_{x'-y'} = 0.012$ directly reflects the C_{2v} symmetry of the growth sequence with planes of specific interface bonds As=Al and Sb=In in the X' plane, and only bulk bonds In–As and Al–Sb in the Y' plane [2]. Interestingly, the birefringence is weakly dispersive. We calculate a slightly larger birefringence for the (InAs)1/(AlSb)1 monolayer superlattice that experiences the maximum C_{2v} symmetry (in this case, the distinction between bulk and interface bonds is meaningless). Conversely, the in-plane anisotropy decreases rapidly when the USPSL cell increases and the interface bond contribution is diluted in a larger contribution of unstrained bulk bonds.

D2d-symmetric superlattices can be obtained from the nominal C2v symmetric (InAs)n/(AlSb)n by substituting Antimony to Arsenic at the first interface of the nominal growth sequence, or by substituting As to Sb at the second interface. We shall denote these USPSLs as 'n/n, 2Sb' and 'n/n, 2As' respectively. As first discussed in Ref. [2], such substitution may allow an enhanced optical anisotropy between the Z and in-plane polarizations (obviously,

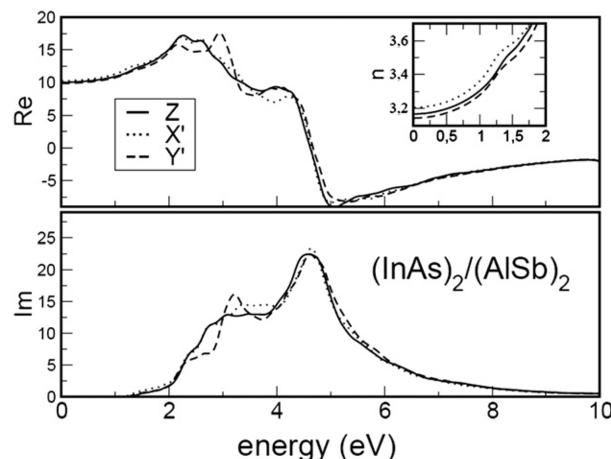

Fig. 5. Calculated imaginary and real part of the dielectric function in a InAs/AlSb 2/2 SL. As predicted from the C2v symmetry, values for polarization along the three eigenaxis Z, X' and Y' differ.

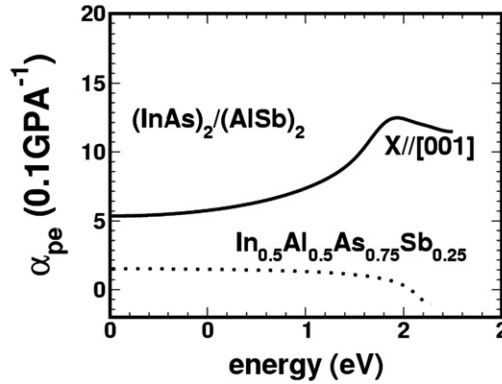

Fig. 6. Comparison of piezo-optic constants in the InAs/AlSb 2/2, 2As Sl and in the cubic quaternary alloy of equivalent stoichiometry. An enhancement far above the maximal value of bulk III–V's is observed for the USPSL.

$\delta n_{x'-y'} = 0$ for D2d symmetry) especially for the common-As interfaces: keeping the in-plane lattice parameter of GaSb, we get $\delta n_{z-x'} = -0.106$ for the '2/2, 2As' SL. An open theoretical question is how the USPSL birefringence is formed. To investigate this point, we compare in Fig. 6 the photo-elastic response of '2/2, 2As' with that of the (cubic) $In_{0.5}Al_{0.5}As_{0.75}Sb_{0.25}$ alloy defined in the virtual crystal approximation. The free standing superlattice has a small native anisotropy $\delta n_{z-x'} = -0.05$ and a very large piezo-optic constant exceeding that of any bulk III–V material. Combining the native anisotropy and piezo-birefringence due to epitaxial strain on a GaSb substrate explains the above mentioned value, $\delta n_{z-x'} = -0.106$. It is also instructive to compare this value with a layer-per-layer average of the piezo-birefringences experienced by the various materials, under same epitaxial strain, $\delta n^{\mathrm{Av}}_{z-x'}$ given for "n/n, 2As" by the simple formula:

$$\delta n^{\mathrm{Av}}_{z-x'} = \delta n^{\mathrm{Av}}_{z-y'} = \big\{(2n-1)\big(\delta n^{\mathrm{InAs}}_{z-x'} + \delta n^{\mathrm{AlSb}}_{z-x'}\big) + 2\delta n^{\mathrm{AlAs}}_{z-x'}\big\}/4n \tag{1}$$

$\delta n^{\mathrm{CA}}_{z-x'}$ ($= \delta n^{\mathrm{CA}}_{z-y'}$) is the piezo-birefringence of material constituent CA under biaxial strain, which can be approximated using $\delta n^{\mathrm{CA}}_{z-x'} \cong C_{11}\varepsilon_{xx}\alpha/2n_0$, where C_{11}, ε_{xx}, α, and n_0 are respectively the elastic stiffness constant, in-plane lattice mismatch, piezo-optic constant, and optical index of bulk CA. For '2/2, 2As' grown on a GaSb substrate, $\delta n^{\mathrm{AlAs}}_{z-x'} = -0.25$ and we obtain $\delta n^{\mathrm{Av}}_{z-x'} = -0.06$. It is interesting to point that the simple formula Eq. (1) also gives the correct sign and order of magnitude for the native anisotropy of the free standing SL.

In summary, the birefringence of '2/2, 2As' under epitaxial strain results from combination of a native anisotropy and an enhanced piezo-birefringence. Clearly, the large local strain at interfaces plays a prominent role. This effect depends crucially on the interface stoichiometry and would be dramatically affected by anion exchange phenomena. On the contrary, the optical anisotropy of C2v-asymmetric $In_{0.5}Ga_{0.5}As$/GaP or $In_{0.5}Ga_{0.5}As$/AlP n/n USPSLs grown on a GaAs substrate is likely to be more robust, as these materials are nearly lattice-matched to GaAs and interface bonds are unstrained. Here, optical anisotropy mainly depends on the birefringence properties of InGaAs and AlP (or GaP) layers. The complex dielectric functions of $In_{0.5}Ga_{0.5}As$/GaP 3/3 for light polarized parallel and perpendicular to the SL direction are shown in Fig. 7. This SL is characterized by a Γ-like conduction-band minimum localized in the $In_{0.5}Ga_{0.5}As$ well and a heavy-hole like valence-band maximum also Γ-like and localized in the $In_{0.5}Ga_{0.5}As$ well. Thus, the lowest-energy interband transition, found at 1.8 eV is direct both in momentum and real space. The material would present a very large transparency domain allowing use of near infrared pump lasers for non-linear optics applications. The calculated birefringence is $\delta n_{z-x'} = -0.06$ and $\delta n_{z-x'} \approx \delta n_{z-y'}$ results from unstrained interfaces that strongly lower C_{2v}-like optical properties. We also found similar results for $In_{0.5}Ga_{0.5}As$/AlP 3/3 lattice-matched to GaAs.

Finally, the calculated TE/TM optical anisotropy of $In_{0.5}Ga_{0.5}As$/AlP n/n grown on GaAs is compared with the averaged piezo birefringence $\delta n^{\mathrm{Av}}_{z-x'}$ in Table 2 using a formula similar to Eq. (1):

$$\delta n^{\mathrm{Av}}_{z-x'} = \delta n^{\mathrm{Av}}_{z-y'} = (2n-1)\big(\delta n^{\mathrm{InGaAs}}_{z-x'} + \delta n^{\mathrm{AlP}}_{z-x'}\big)/4n \tag{2}$$

The observed agreement evidences that quantum confinement effects play a weaker role in this system, where birefringence mainly derives from averaging $In_{0.5}Ga_{0.5}As$ and AlP piezo-birefringences. In other words, in this system,

Table 2
Calculated birefringence of $In_{0.5}Ga_{0.5}As/AlP$ n/n USPSLs grown on a GaAs substrate

	$n=1$	$n=2$	$n=3$
$\delta n_{z-x'}$	-0.048	-0.055	-0.059
$\delta n_{z-x'}^{\mathrm{Av}}$	-0.045	-0.067	-0.081

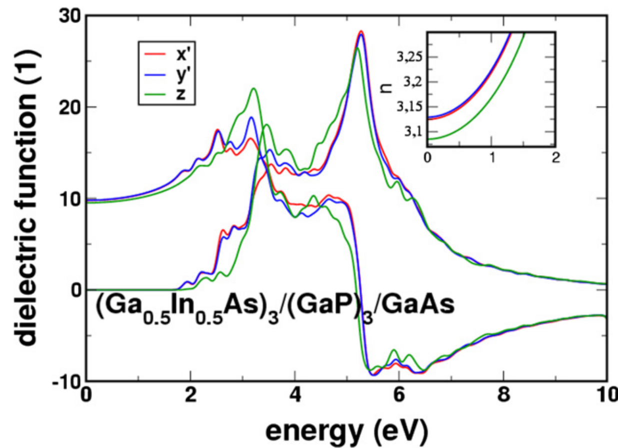

Fig. 7. Calculated dielectric function (real and imaginary parts) for the $In_{0.5}Ga_{0.5}As/GaP$ 3/3 SL.

built-in strains compensate each other and give a free-standing SL lattice-matched to GaAs, but piezo-birefringences do not compensate because of the large difference in piezooptic constants. This results in a large native birefringence, which increases with the superlattice period since, as n increases, a larger fraction of strained bonds contribute to the overall result. That complex spectral features observed in Figs. 5, 7 can be summarized with such a simple 'rule of thumb' as the averaging of piezo-birefringence is a rather astonishing and remarkable result.

5. Experimental attempts: MBE growth of NCA USPSLs

In view of the promising $\delta n_{z-x'} = 0.106$, an initial attempt was made to grow InAs/AlSb 'n/n, 2As' superlattices using MBE. Clearly, anion exchange when commuting the group V elements could be avoided only if unusually low temperature conditions were chosen. In practice, temperatures of the order of 400 °C were used instead of the usual 550 °C. The first issue was checking the possibility of an effective control of interface stoichiometry using shutter manipulations and growth interruption sequences. The TEM cross-section of a InAs/AlSb 'n/m, 2 As' shown in Fig. 8 shows perfectly symmetric interfaces marked by dark lines characteristic of the AlAs half-monolayers. Similar structures grown without special manipulations show clearly asymmetrical interfaces. The second problem is the large strain with respect to a GaSb substrate: for instance, the 2/2, 2 As SL has a free-standing lattice parameter equal to 5.97 Å, which is about 2% smaller than that of GaSb: only a few periods can be grown before plastic relaxation starts. In order to grow thick heterolayers, it is necessary to introduce strain-compensation layers (hoping that their intrinsic piezo-birefringence will not compensate completely the SL birefringence). In this attempt, 16 monolayer thick AlInSb layers were intercalated with 4-period '2/2, 2As' SL sequences. The TEM cross-section displayed in Fig. 9 shows that the thin layers are locally well defined, but large oscillations of the interfaces are observed, which destroy the long range order and actually prevent an atomic resolution study. The development of significant interface roughness probably associated with partial phase separation was observed in nearly all our attempts to grow tensile-strained layers with large mismatch ($>2\%$). We note here that the growth of tensile strained layers was far less studied than that of compressively strained layers, and a strong asymmetry between these two configurations is revealed by the present study. Guided-wave optical measurements at $\lambda = 1.5$ μm were attempted in a structure similar to that in Fig. 9, having AlGaSb optical confinement layers. They revealed, unexpectedly, a good transmission of the TM mode and a strong absorption of the TE mode, which was possibly due to free carrier absorption.

Fig. 8. TEM cross-section of a InAs/AlSb ‘n/m, 2 As’ with relatively thick layers. The interfaces are clearly symmetric and underlined by the dark lines corresponding to AlAs half-monolayers.

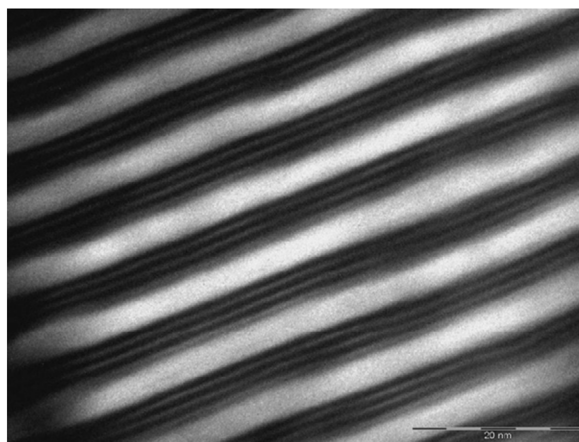

Fig. 9. TEM cross-section of a InAs/AlSb 2/2, 2As SL. Groups of 4 period SL are separated by AlAsSb strain compensation layers (light grey). The layers are locally well defined, but large oscillations of the interfaces destroy the long-range order.

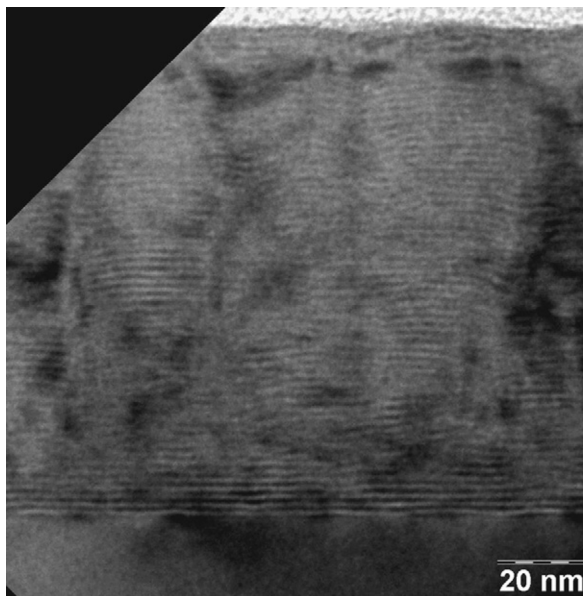

Fig. 10. TEM cross-section of a GaP/GaInP 3/3 SL lattice matched to GaAs. Large oscillations of interfaces and extended defects are observed.

While proving the feasibility of interface control and ultrathin layer growth, the results on the InAs/AlSb system are not completely encouraging, due to the need for strain compensation layers and also because the superlattice itself remains a small gap material not suitable for optical pumping with conventional near infrared lasers. These drawbacks are absent in the GaInAs–GaP or GaInAs–AlP systems on which we focused subsequent effort. The TEM cross-section of a GaInAs/GaP 3/3 SL shown in Fig. 10 illustrates the difficulty of obtaining plane interfaces: while the succession of 3 monolayers is visible at a local scale, large interface oscillation and roughness develop, and a number of extended defects appear. From the expertise in InGaAs epitaxial growth, we concluded that tensile strained GaP was most probably responsible for this behavior: the high surface mobility of Ga allows strain relaxation via thickness oscillations (alternating thin highly strained regions and thicker, less strained regions) precursory to a transition towards a 3-D growth mode. This conclusion suggested the substitution of Al for Ga, since Al is known for its very low surface mobility. The TEM cross-section of a $In_{0.5}Ga_{0.5}As$/AlP 3/3 USPSL shows the success of this ultimate attempt: despite the huge ($\pm 3.5\%$) strain stored in individual layers, atomically flat interfaces are observed over large areas, to

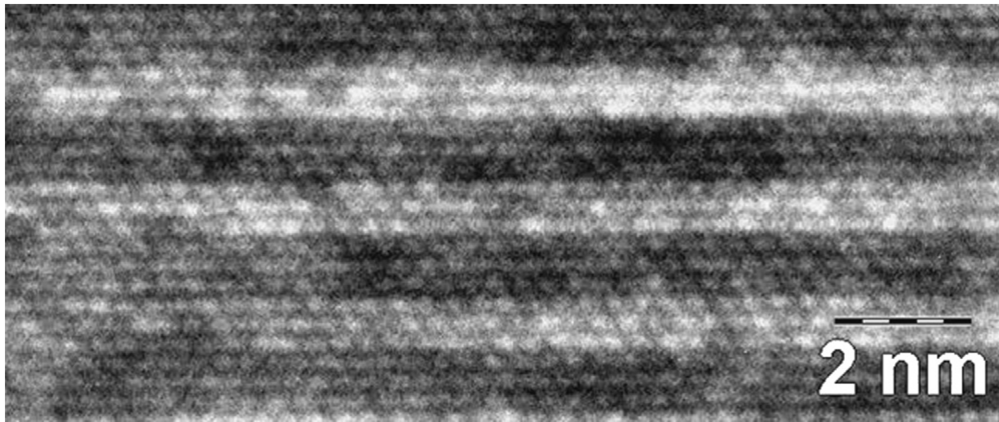

Fig. 11. TEM cross-section of a GaInAs/AlP 3/3 SL lattice matched to GaAs. Strains are equivalent to that in Fig. 10, but the low surface mobility of Al atoms hampers the phase separation and prevents transition to a three-dimensional growth mode.

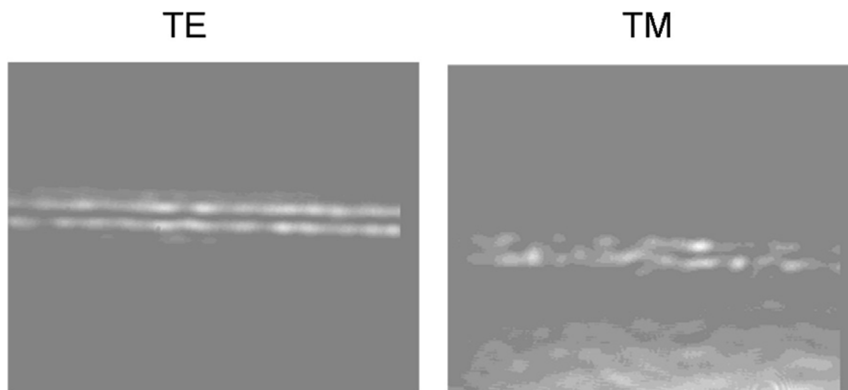

Fig. 12. Intensity profile of both guided modes at $\lambda = 1.5$ μm in a 1000 μm-long plane waveguide consisting of a 400 nm thick GaInAs/AlP 3/3 SL embedded between 2 μm-thick $Al_{0.85}Ga_{0.15}As$ cladding layers. Injected light is TE/TM polarized.

such an extent that X-ray diffraction using a double monochromator apparatus (that tests a huge coherence volume) clearly reveals the supercell structure with exactly 6 monolayers. This sample gives a weak luminescence signal at 1.6 eV, in fair agreement with expectation. A 400 nm (236 period) thick superlattice embedded between 2 μm thick $Al_{0.85}Ga_{0.15}As$ optical confinement layers was grown[1] for guided-wave optical measurements. The intensity profile at the output facet of a 1000 μm long plane waveguide, shown in Fig. 12, reveals the fair transparency, observed both in TE and TM polarizations. Unfortunately, the observed split-line demonstrates a problem with this waveguide, which seems to be the coexistence of an Anti Resonant Reflecting Optical Waveguide (ARROW) mode [15] with the expected index-guided mode. FDTD simulation using calculated values of the indices confirm this coexistence. The coupling of these two modes makes group index measurement meaningless and do not allow concluding on the SL optical anisotropy.

6. Conclusion

In summary, we have reported an original attempt to implement birefringence in zinc-blende based artificial semiconductors consisting of ultra-short period superlattices of highly strained materials sharing no-common atom. Surprisingly, the complex results of atomistic calculations of the dielectric function can, in many cases, be explained and approximated in terms of layer-by-layer averaging of the piezo-birefringences experienced by the different host

[1] This corresponds to a 10 hour MBE run, due to the required growth interruption time at each interface.

materials. At least one of the possible material combinations fulfilling the large number of requirements for practical use in the context of non-linear optics could be grown with remarkably high crystalline integrity. Further studies are still needed to validate the theoretical predictions concerning the optical anisotropy of these materials. Finally, it would be quite interesting to use the same advanced tight-binding method and calculate second order susceptibilities. This should be a straight forward (albeit computationally difficult) extension of the formalism that would allow a search for optimization of the second order non-linearity in artificial materials such as USPSLs.

Acknowledgement

The authors would like to thank Drs. Rita Magri and Angela Vasanelli for their participation to the early stage of this work.

References

[1] J.A. Armstrong, N. Blombergen, J. Ducuing, P.S. Pershan, Phys. Rev. 127 (1962) 1918.
[2] J.-M. Jancu, A. Vasanelli, R. Magri, P. Voisin, Phys. Rev. B 69 (2004) 241303R.
[3] J.-M. Jancu, R. Scholz, F. Beltram, F. Bassani, Phys. Rev. B 57 (1998) 6493.
[4] S. Cortez, O. Krebs, P. Voisin, Eur. Phys. J. B 21 (2001) 241 and ref. therein.
[5] L. Ivchenko, A. Kaminski, U. Rössler, Phys. Rev. B 54 (1996) 5852.
[6] B. Foreman, Phys. Rev. Lett. 81 (1998) 425.
[7] R. Magri, S. Ossicini, Phys. Rev. B 63 (2001) 165303.
[8] A.V. Platonov, V.P. Kochereshko, E.L. Ivchenko, G.V. Mikhailov, D.R. Yakovlev, M. Keim, W. Ossau, A. Waag, G. Landwehr, Phys. Rev. Lett. 83 (1999) 3546.
[9] O. Madelung (Ed.), Semiconductors: Group IV Elements and III–V Compounds, Landolt–Börnstein New Series, Group III, Pt. a, vol. 17, Springer, Berlin, 1982;
O. Madelung (Ed.), Semiconductors: Intrinsic Properties of Group IV Elements and III–V, II–VI and I–VII Compounds, Landolt–Börnstein New Series, Group III, Pt. a, vol. 22, Springer, Berlin, 1987.
[10] B. Boykin, P. Vogl, Phys. Rev. B 64 (2002) 3502.
[11] B. Arnauld, M. Alouani, Phys. Rev. B 63 (2001) 85208.
[12] R. Magri, unpublished calculations.
[13] K.A. Mader, A. Zunger, Phys. Rev. B 50 (1994) 17393.
[14] S. Botti, N. Vast, L. Reining, V. Olevano, L.C. Andreani, Phys. Rev. Lett. 89 (2002) 216803.
[15] D. Yin, J.P. Barber, A.R. Hawkins, D.W. Deamer, H. Schmidt, Appl. Phys. Lett. 85 (2004) 3477.